Effects of Sodium Sulphide as an Inhibitor on CdS Films Obtained by Chemical Bath Deposition

M. Önal and B. Altiokka

Bilecik Seyh Edebali University, 11210, Bilecik, Turkey

In the present study, CdS thin films were produced on glass substrates by the chemical bath deposition method, and sodium sulfite was used to reduce the reaction rate. Based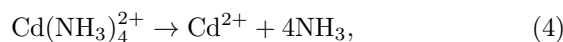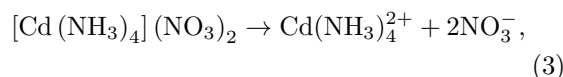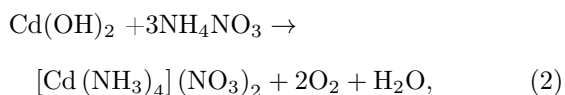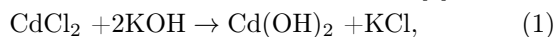 on the absorbance measurements, it was found that the energy band gaps of the films increased from 2.35 to 2.49 eV depending on the amount of inhibitor. It was also found that when the reaction rate decreased, the crystal structure of the films shifted from the cubic phase to the hexagonal phase in reference to the X-ray diffraction results. When CdS thin films had the hexagonal phase, it was seen in the scanning electron microscope images that pinholes and voids were not seen on the surface of the films. Surface roughness values were calculated using scanning electron microscope images, and these values were found to vary between 22 nm and 9 nm.

topics: chemical bath deposition, thin films, CdS, inhibitor

1. Introduction

Cadmium sulfide (CdS) is an II–VI compound semiconductor material with cubic (zincblende) and hexagonal (wurtzite) crystal systems with a wide band gap of about 2.42 eV at room temperature [1, 2]. CdS thin films have many applications in optoelectronics, such as tunable light-emitting diodes, photo sensors, piezoelectric transducers, laser materials, and nonlinear integrated optical devices. In addition, CdS has notable photovoltaic properties for thin-film heterojunction solar cells as it has both the best lattice and thermal expansion matching for $CuInSe_2$ and CdTe films [3]. Chemical bath deposition (CBD) is easy to apply, does not require complex systems, and is low in cost. Besides, it attracts the attention of researchers due to its possibility to change the size of the grains depending on the solution conditions and to obtain thin films with a large surface area at low temperatures. One of the other advantages of this technique is that it can be controlled to deposit uniform thin films [4]. One of the ideal methods for the growth of large-area thin films at temperatures below 100°C is the chemical surface deposition (CSD) method [5].

The equations showing the chemical processes in the production of cadmium sulfate by chemical bath deposition method are given as follows [6]

$$CdCl_2 + 2KOH \rightarrow Cd(OH)_2 + KCl, \tag{1}$$

$$Cd(OH)_2 + 3NH_4NO_3 \rightarrow$$
$$[Cd(NH_3)_4](NO_3)_2 + 2O_2 + H_2O, \tag{2}$$

$$[Cd(NH_3)_4](NO_3)_2 \rightarrow Cd(NH_3)_4^{2+} + 2NO_3^-, \tag{3}$$

$$Cd(NH_3)_4^{2+} \rightarrow Cd^{2+} + 4NH_3, \tag{4}$$

$$CS(NH_2)_2 + 2H_2O \rightarrow 2NH_3 + CO_2 + H_2S, \tag{5}$$

$$H_2S \rightarrow S^{2-} + 2H^+, \tag{6}$$

$$Cd^{2+} + S^{-2} \rightarrow CdS. \tag{7}$$
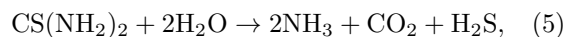
When the literature was searched for the production of CdS thin films, no studies were found on reducing the reaction rate by using Na_2SO_3. However, there were two studies on the inhibitory effects of Na_2SO_3. These studies were related to ZnS thin films obtained by the electrodeposition method and PbS thin films obtained by the CBD method. In mentioned studies on ZnS and PbS, good crystalline and pinhole-free films could be obtained by using inhibitors of Na_2SO_3 [7, 8]. Therefore, the use of inhibitors was recommended [8].

In our study, CdS thin films were obtained by the CBD technique. During production, Na_2SO_3 was used as an inhibitor for the first time, and the effects of the reaction rate were investigated in detail. In the literature, there was no prior study using Na_2SO_3 for CdS production. The use of varying amounts of Na_2SO_3 decreased the reaction rate for CdS. Besides, hexagonal phases were obtained by using an inhibitor without annealing. The band gaps of the films were increased from 2.35 to 2.49 eV depending on the amount of Na_2SO_3. Additionally, the use of inhibitors provided pinhole-free and crack-free films. All these results are important

Experimental parameters.

Exp.	CdCl$_2$ [g]	KOH [g]	NH$_4$(NO)$_3$ [g]	Thiourea total [g]	Na$_2$SO$_3$ [g]	Deposition time [min]
RR0	0.05	0.9	1.3	0.23	0.0000	300
RR1	0.05	0.9	1.3	0.23	0.0025	300
RR2	0.05	0.9	1.3	0.23	0.0050	300
RR3	0.05	0.9	1.3	0.23	0.0075	300
RR4	0.05	0.9	1.3	0.23	0.0100	300

because of the fact that hexagonal phases and relatively high band gaps are preferred for solar cells. In order to obtain higher efficiency from solar cells, a hexagonal buffer layer is preferred over a cubic structure due to the higher optical band gap. The CdS with a polymorphic structure shows piezoelectricity, while the hexagonal structure shows pyroelectricity [9].

2. Experimental details

The CBD technique was preferred for depositing CdS thin films on glass substrates. First, the bath container and glass substrates were carefully washed with 5% hydrochloric acid and rinsed with deionized water. In all experiments, 0.05 g of cadmium chloride (CdCl$_2$), 0.9 g of potassium hydroxide (KOH), 1.3 g of ammonium nitrate (NH$_4$NO$_3$), and 0.23 g of thiourea (CH$_4$N$_2$S) were dissolved in 100 ml of deionized water, respectively. And the pH value of the solutions was adjusted to 9.5 using ammonia. The solutions were stirred at 800 rpm. After the pH values were adjusted, the solutions were heated up to 85°C. In a previous study, CdS formation was shown to be completed in an average of 200 min [10]. Therefore, for all samples, the deposition time was chosen to be 300 min. During this period, the thicknesses of all samples reached approximately the same value. This situation leads us to conclude that the reaction was over. The samples were named RR0, RR1, RR2, RR3, and RR4 depending on the used amount of Na$_2$SO$_3$, which was 0, 2.5, 5.0, 7.5, and 10 mg, respectively. The sample surfaces were rinsed with pressurized deionized water to clean the chemical residues and left to dry at room temperature. Summarized experimental details are given in Table I.

The gravimetric method was used to determine the film thickness of the samples. Fourier transform infrared (FTIR) spectroscopy studies were used to investigate the chemical structure of the thin films and to determine the existence of hydroxyl groups and/or other compounds in the obtained CdS films [11]. A PerkinElmer FTIR device was used for Fourier transform analysis. The crystal structures of the samples were investigated using PANalytical Empyrean X-ray diffractometer, A&E LAB UV-vis instrument was used to determine their
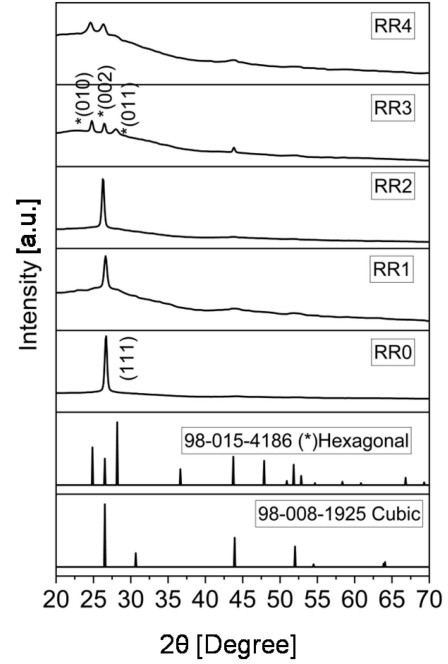

Fig. 1. X-ray diffraction pattern of CdS formed depending on the amount of inhibitor.

optical properties, and surface morphology was determined with a Zeiss SUPRA 40VP scanning electron microscope.

3. Result and discussion

3.1. Structural analysis of CdS films

Thickness analysis of the produced thin films was done using the gravimetric method, and the related equation is given as [12]

$$t = \frac{m}{\rho A}. \qquad (8)$$

In (8), the thickness of the film is represented by t, mass by m, and the surface area by A, while ρ represents the density of CdS, which is 4.84 g/cm^3 [13]. The thicknesses of the films obtained in RR0, RR1, RR2, RR3, and RR4 were 360, 345, 355, 330, and 325 nm, respectively. Standard deviation (SD) and uncertainty (U) were calculated like in the previous

TABLE II

Calculated crystallite size and band gaps of CdS thin films.

Exp.	cs [nm] (111) cubic	cs [nm] (010) hexagonal	cs [nm] (002) hexagonal	cs [nm] (011) hexagonal	cs [nm] average	Band gap [eV]
RR 0	26	–	–	–	26	2.35
RR 1	18	–	–	–	18	2.39
RR 2	22	–	–	–	22	2.35
RR 3	–	25	27	17	23	2.47
RR 4	–	24	16	–	20	2.49

TABLE III

The full width at half maximum (FWHM), diffraction angle 2θ, Miller indices (hkl), inter planar spacing (d), and lattice constants (a and c).

Exp.	FWHM	2θ	hkl	d [Å]	Calc. a [Å]	Calc. c [Å]	Ratio c/a
RR 0	0.3463	26.703	(111)	3.34234	5.789		
RR 1	0.4344	26.614	(111)	3.34804	5.798		
RR 2	0.361	26.250	(111)	3.39058	5.872		
RR 3	0.370	24.773	(010)	3.59460	4.150		
	0.372	26.435	(002)	3.37046		6.740	1.624
	0.587	27.998	(011)	3.18765			
RR 4	0.585	24.593	(010)	3.61958	4.179		
	0.568	26.338	(002)	3.38813		6.776	1.621

Cubik phase ASTM card number 98-008-1925; $a = b = c = 5.83$ Å

Hexagonal phase ASTM card number 98-015-4186; $a = b = 4.137$ Å, $c = 6.716$ Å

study [14]. According to this calculation, the standard deviation was determined as 15.2 nm and the uncertainty as 6.8 nm. Therefore, it can be said that the thicknesses of the films were nearly the same.

The patterns of the samples obtained from X-ray diffractometry are given in Fig. 1. The chosen 2θ scanning range was between 20–70°. When the X-ray diffraction (XRD) patterns were examined, it was seen that the films obtained in RR0, RR1, and RR2 had a cubic structure, while the films obtained in RR3 and RR4 had a hexagonal structure, depending on the reaction rate. In the comparison made using the ASTM cards numbered 98-008-1925 and 98-015-4186, it was observed that the first three samples had a single peak belonging to the cubic structure in the (111) plane. Other samples were formed in the hexagonal phase. This is important due to the fact that CdS with hexagonal phases have a more stable structure than the cubic structure [15]. The peaks of the cubic structure were around $2\theta = 26.7(111)$ degrees, and the hexagonal peaks were found to be at $2\theta = 24.86(010)$, $26.52(002)$, and $28.17(011)$ degrees.

Scherrer's equation, in which the average crystallite sizes (cs [nm]) are calculated using the full width of half maximum (FWHM) values, is given as

$$\text{cs} = \frac{0.089 \times 180\lambda}{314\,\beta\cos(\theta_C)}. \tag{9}$$

The symbols used in this equation are: λ — the wavelength of X-ray radiation (1.54056 Å), β — FWHM, and θ_C — the Bragg diffraction angle [16]. The calculated average crystallite sizes are presented in Table II. According to Table II, the crystallite sizes were between 18 and 26 nm.

The lattice parameters for cubic structure and hexagonal structure were calculated using, respectively,

$$a = d\sqrt{\left(h^2 + k^2 + l^2\right)}, \tag{10}$$

and

$$\frac{1}{d_{(hkl)}^2} = \frac{4}{3}\left(\frac{h^2 + hk + k^2}{a^2}\right) + \frac{l^2}{c^2}, \tag{11}$$

where $d = d_{(hkl)}$ is the interplanar spacing, (hkl) is the Miller indices, a and c are the lattice parameters, respectively [12]. The crystallographic parameters given in the ASTM cards used are $a = b = c$ (5.83 Å) for cubic structure and $a = b$ (4.137 Å) and c (6.716 Å) for hexagonal structure. It was seen that the calculated lattice constant values were almost the same as the crystallographic parameters given in the ASTM cards, especially the c/a value for the hexagonal structure exactly matched. The full width at half maximum (FWHM), diffraction
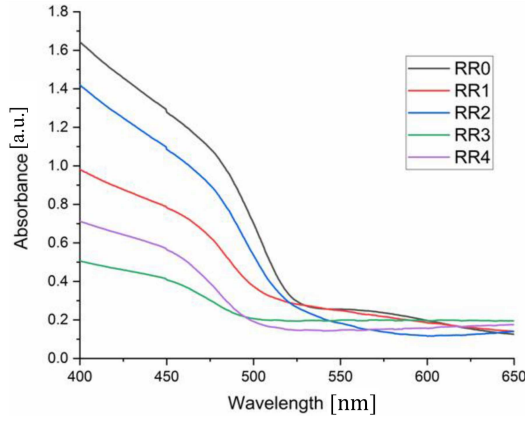
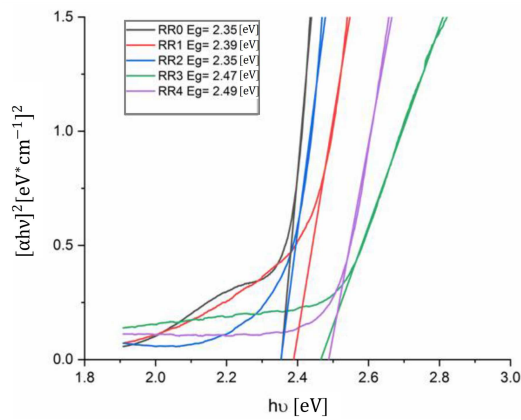Fig. 2. Absorbance measurements of CdS thin films.

Fig. 3. Energy band gaps of CdS thin films depending on the reaction rate.

angle 2θ, Miller indices (hkl), interplanar spacing (d), and lattice constants (a and c) are given in Table III.

3.2. Optical properties of the CdS films

The optical properties of the CdS thin films were investigated by absorbance measurements versus wavelength and are given in Fig. 2. When the absorbance graphs were analyzed, it was noticed that when the sharp increase was observed at about 500 nm in the samples named RR3 and RR4, the sharp increase was also observed around 550 nm in the samples named RR0, RR1, and RR2. The fact that all absorbance lines were at the same level at 650 nm wavelength indicated that the film thicknesses approximately had the same value. Besides, high absorbance is not preferred for the window layer since the high absorbance absorbs the rays from the sun and prevents them from reaching the junction area. A low absorption value is preferred for materials used as a window layer in the solar cell [17].
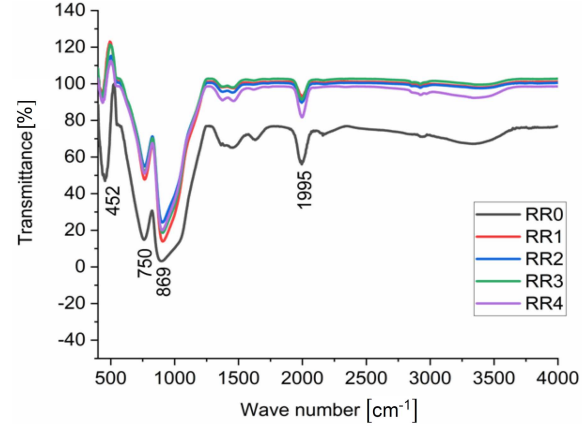

Fig. 4. FTIR spectra of CdS thin films.

The energy band gap values of the samples were estimated using Tauc plots, and these values are presented in Fig. 3. Tauc plot is represented by

$$(\alpha h\nu) = B\left(h\nu - E_g\right)^n. \tag{12}$$

In (12), for allowed direct transitions, $n = 1/2$, E_g is the energy band gap, $h\nu$ is the photon energy, and B is a constant [18]. The band gap is estimated from the point where the $(\alpha h\nu)^2$ graph intersects the $h\nu$ axis ($h\nu = 0$). Figure 3 shows that the energy band gaps of the films obtained in RR0, RR1, and RR2 varied between 2.35 and 2.39 eV. The energy band gaps of the films are also given in Table II. The energy band gap of CdS thin films produced at 85°C is 2.38 eV, according to the literature [19]. The energy gaps of the films obtained in RR0, RR1 and RR2 matched the values stated in the literature for films with cubic structures. It is known that the energy band gaps of CdS thin films with hexagonal structures are 2.58 eV [15]. Therefore, it can be said that the band gap values of 2.47 eV and 2.49 eV of the films obtained in RR3 and RR4 are suitable for use in solar cells.

3.3. FTIR of the CdS films

In this study, the FTIR values were recorded at wave numbers in the range of 400–4000 cm^{-1} and are given in Fig. 4. Metal oxides show absorption bands below 1000 cm^{-1} resulting from interatomic vibrations. The two peaks at 750 cm^{-1} and 869 cm^{-1} in Fig. 4 are assigned to the stretching frequency of the Cd–S bond [20]. The peak around 1995 cm^{-1} is due to the presence of (carbon–nitrogen) C–N stretching vibration of cyanamide or thiocyanate, which is formed by the chemical reaction of the thiourea and ammonia [21]. Figure 4 shows that there was a remarkable increase in the transmittance values of the samples produced using the inhibitor. This can be attributed to the reduction in crystal defects due to the use of the inhibitor [22].
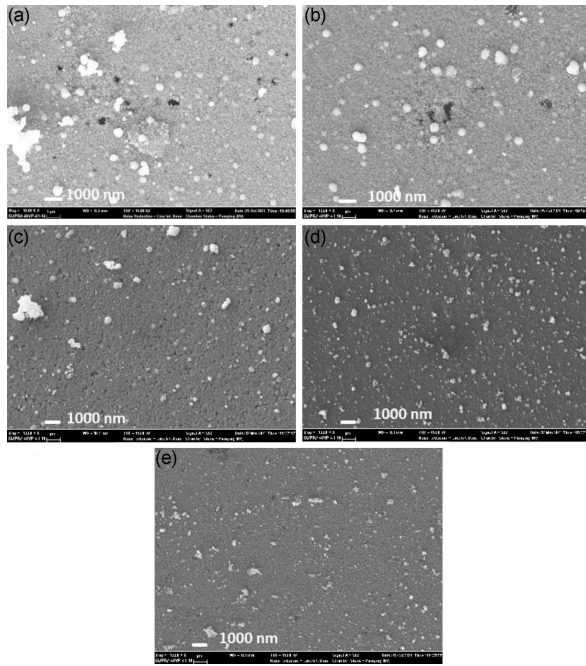
Fig. 5. SEM images of CdS thin films at $10k\times$ magnification, obtained for (a) RR0, (b) RR1, (c) RR2, (d) RR3, (e) RR4.
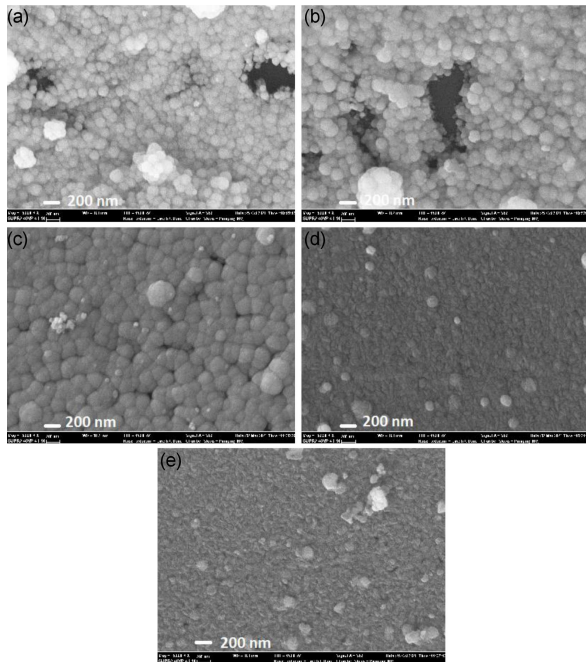

Fig. 6. SEM images of CdS thin films at $50k\times$ magnification, obtained for (a) RR0, (b) RR1, (c) RR2, (d) RR3, (e) RR4.

3.4. SEM analysis of the CdS films

Scanning electron microscope (SEM) images were obtained to analyze the surface morphology of CdS thin films produced on glass substrates. In order to visualize all pinholes and voids, SEM images of the
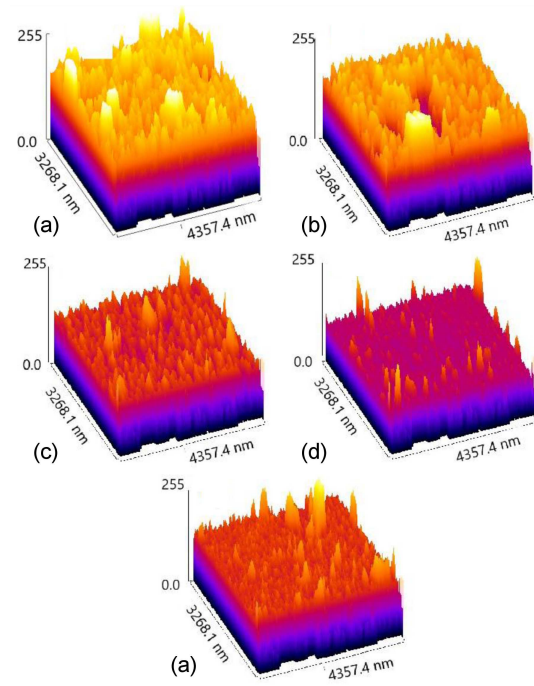

Fig. 7. Surface roughness plots of CdS thin films obtained in (a) RR0, (b) RR1, (c) RR2, (d) RR3, (e) RR4.
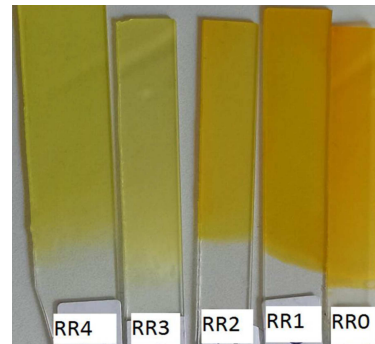

Fig. 8. Photograph of CdS films.

samples were taken at $10k\times$ magnification as well as $50k\times$ magnification in our study. The $10k\times$ magnified SEM images are given in Fig. 5. According to Fig. 5, there were plenty of pinholes and cracks on the surface of films obtained in RR0, RR1, and RR2. Films obtained in RR3 and RR4, on the contrary, had hexagonal phases, and there were no pinholes and cracks on the surface of the films. It was observed that the surfaces of these two films were quite homogeneous and compact at both $10k\times$ magnification and $50k\times$ magnification. It is important because of the fact that pinholes can cause short circuits in solar cells.

The $50k\times$ magnified images are given in Fig. 6. According to Fig. 6, there are no pinholes and voids on the surface of the films, which have hexagonal phases.

TABLE IV

Surface roughness values calculated with ImageJ software.

Exp.	Na$_2$SO$_3$ [g]	Ra [nm]	Rq [nm]
RR 0	0.0000	22	27
RR 1	0.0025	21	26
RR 2	0.0050	12	16
RR 3	0.0075	9	12
RR 4	0.0100	11	14

The surface roughness of the samples was analyzed by processing SEM images with ImageJ software. There are many studies in the literature in which surface morphology analysis was performed using ImageJ software [1, 23, 24]. The roughness images are given in Fig. 7, and roughness values are presented in Table IV. The surface roughness of the obtained films with the cubic structure was considerably higher than that of the films with the hexagonal structure. As can be seen in Table IV, the average roughness values changed from RR0 to RR4 to 22, 21, 12, 9, and 11 nm, respectively. This result was notable because of the fact that the roughness values of the hexagonal phase were quite low. Therefore, it can be said that the transmittance values were high, and at the same time, they are in line with the literature [25].

3.5. Visual analysis of the CdS films

The photograph of the samples is given in Fig. 8. As seen in this photograph, CdS adhered very well to the glass substrates, and they were homogeneous. There were no voids or defects on the surfaces of all samples. There were differences in the color tones of the samples, as seen in the photograph. The shift of the crystal from the cubic phase to the hexagonal phase might have caused this color tone difference.

4. Conclusions

In this study, the chemical bath deposition method was employed to grow the CdS thin films. While the CdS thin films were produced, Na$_2$SO$_3$ was used as an inhibitor for the first time, and its effects were investigated. Thicknesses measurement showed that the film thicknesses varied between 360 and 320 nm. There were no remarkable differences in the thicknesses of the samples. XRD patterns showed that when the reaction rate decreased, the phase of the films shifted from cubic to hexagonal. It was a remarkable result due to the fact that the hexagonal structure of CdS was more stable than the cubic structure. The energy band gap values were estimated using the Tauc plots, and they showed that the band gaps of the films increased from 2.35 to 2.49 eV as the reaction duration increased by using Na$_2$SO$_3$. SEM images were used to analyze the surface morphologies of the films. When the reaction rate was decreased, pinholes and cracks were not seen on the surface of the films with hexagonal phases. It was found that the surface roughness values were between 22 and 9 nm, and the surface roughness values of the films obtained with the hexagonal structure were lower than that with the cubic structure. These values were critical due to the fact that low surface roughness causes high transmittance for solar cells.

References

[1] S.J. Ikhmayies, *JOM* **73**, 1261 (2021).

[2] S.J. Ikhmayies, *JOM* **69**, 144 (2017).

[3] S.J. Ikhmayies, *JOM* **66**, 46 (2014).

[4] A. Tanushevski, H. Osmani, *Chalcogenide Lett.* **15**, 107 (2018).

[5] G.A. Il'Chuk et al., *Inorg. Mater.* **50**, 762 (2014).

[6] M. Önal, B. Altıokka, *Emerg. Mater. Res.* **9**, 738 (2020).

[7] M. Society, *J. Electron. Mater.* **48**, 2398 (2019).

[8] B. Altiokka, M.C. Baykul, M.R. Altiokka, *J. Cryst. Growth* **384**, 50 (2013).

[9] R. Anionye Daniel-Umeri, *Int. J. Mater. Sci. Appl.* **4**, 138 (2015).

[10] E. Çetinörgü, C. Gümüş, R. Esen, *Thin Solid Films* **515**, 1688 (2006).

[11] A.L. Salas-Villasenor, I. Mejia, M. Sotelo-Lerma, B.E. Gnade, M.A. Quevedo-Lopez, *Appl. Phys. Lett.* **101**, 262103 (2012).

[12] I.M.S. Mohammed et al., *Appl. Phys. A Mater. Sci. Process.* **127**, 1 (2021).

[13] S. Hariech, M.S. Aida, J. Bougdira, M. Belmahi, G. Medjahdi, D. Genčve, *J. Semicond.* **39**, 034004 (2018).

[14] H. Arat, O. Arslan, U. Ercetin, A. Akbulut, *Case Stud. Therm. Eng.* **26**, 101117 (2021).

[15] A. Ashok, G. Regmi, A. Romero-Núñez, M. Solis-López, S. Velumani, H. Castaneda, *J. Mater. Sci. Mater. Electron.* **31**, 7499 (2020).

[16] R. Bhowmik, M.N. Murty, E.S. Srinadhu, *PMC Phys. B* **1**, (2008).

[17] K.C. Wilson, E. Manikandan, M.B. Ahamed, B.W. Mwakikunga, *J. Alloys Compd.* **585**, 555 (2014).

[18] O.I. Diaz-Grijalva, D. Berman-Mendoza, A. Flores-Pacheco, R. López-Delgado, A. Ramos-Carrazco, M.E. Alvarez-Ramos, *J. Mater. Sci. Mater. Electron.* **31**, 1722 (2020).

[19] F. Liu et al., *J. Alloys Compd.* **493**, 305 (2010).

[20] M.A. Islam et al., *Opt. — Int. J. Light Electron Opt.* **126**, 3177 (2015).

[21] S.M.M. Muthusamy, *J. Mater. Sci. Mater. Electron.* **23**, 1647 (2012).

[22] S. Chander, M.S. Dhaka, *Thin Solid Films* **638**, 179 (2017).

[23] N.A. Bakr, Z.T. Khodair, A.M. Saleh, *Int. J. Appl. Eng. Res.* **13**, 10796 (2018).

[24] S. Dev, P. Kumar, A. Rani, A. Agarwal, R. Dhar, *Superlattices Microstruct.* **145**, 106638 (2020).

[25] M.J. Kim, H.T. Kim, J.K. Kang, D.H. Kim, D.H. Lee, S.H. Lee, S.H. Sohn, *Mol. Cryst. Liq. Cryst.* **1406**, 20 (2010).